Wave turbulence in a two-layer fluid: Coupling between free surface and interface waves

Bruno Issenmann[1,2], Claude Laroche[1] and Eric Falcon[1]

[1] *Université Paris Diderot, Sorbonne Paris Cité, MSC, UMR 7057 CNRS - F-75013 Paris, France*
[2] *Univ Lyon, Université Claude Bernard Lyon 1, CNRS, Institut Lumière Matière
F-69622, Villeurbanne, France*

Abstract – We experimentally study gravity-capillary wave turbulence on the interface between two immiscible fluids of close density with free upper surface. We locally measure the wave height at the interface between both fluids by means of a highly sensitive laser Doppler vibrometer. We show that the inertial range of the capillary wave turbulence regime is significantly extended when the upper fluid depth is increased: The crossover frequency between the gravity and capillary wave turbulence regimes is found to decrease whereas the dissipative cut-off frequency of the spectrum is found to increase. We explain these observations by the progressive decoupling between waves propagating at the interface and the ones at the free surface, using the full dispersion relation of gravity-capillary waves in a two-layer fluid of finite depths. The cut-off evolution is due to the disappearance of parasitic capillaries responsible for the main wave dissipation for a single fluid.

Introduction. – Stratified fluids are ubiquitous in Nature such as in oceans or in the atmosphere. The density stratification is usually due to a temperature or salinity gradient with the depth in oceans, or a temperature or humidity gradient with altitude in the atmosphere. The simplest stratified fluid consists in two superimposed homogeneous fluids, the fluid with higher density being below the fluid with lower density. In this situation, waves can propagate at the interface between the two fluid layers but also at the free surface of the top one. Under certain conditions, surface and interface waves interact together [1,2]. An astonishing manifestation of this phenomenon is the dead-water effect first observed in 1904 on the sea surface [3], and recently reproduced in experiments [4,5]. Indeed, ships evolving on a calm sea can slow or even stop sailing in a two-layer fluid due to the extra-drag generated by large interface waves. The coupling between the surface and interface waves in a two-layer fluid also generates narrow nested V-shaped wakes observed behind ships [6,7], as well as the damping of ocean surface waves over a layer of fluid mud [8]. Such a coupling is also involved in Faraday instability of floating droplets on a liquid bath [9,10], or during the long-wave instabilities in thin two-layer liquid films ($< 100\,\mathrm{nm}$) in chemical physics [11]. In industrial applications like metal refining, such interactions can also have an influence on the ripples created during dewetting [12]. Finally, the coupling between the surface and interface waves of large amplitudes occur in many physical and biological situations (involving or not elasticity), and lead to numerous challenging studies in applied mathematics such as the predictions of new solitary waves [13,14].

When a set of stochastic waves, propagating on a free surface, has large enough amplitudes, interactions between nonlinear waves can generate a wave turbulence regime. These interactions transfer the wave energy from the large scales, where it is injected, to the small scales where it is dissipated. This generic phenomenon concerns various domains at different scales: Surface and internal waves in oceans, elastic waves on plates, spin waves in solids, magnetohydrodynamic waves in astrophysical plasma (for reviews, see [15–18]). The weak turbulence theory developed in the 1960s [19–21] leads to predictions on the wave turbulence regime in almost all domains of physics involving waves [16,17]. The past decade has seen an important experimental effort to test the validity domain of the weak
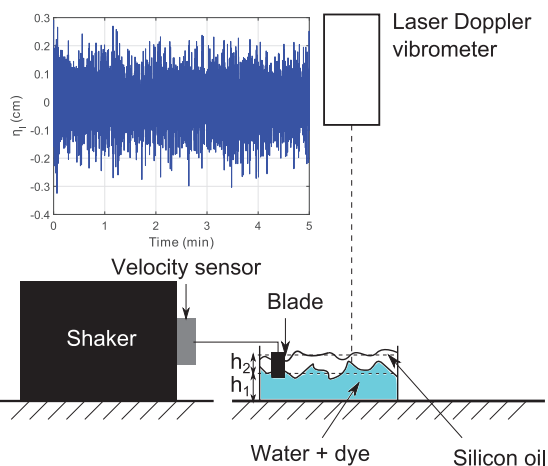
Fig. 1: (Color online) Experimental setup. Free surface and interfacial waves are generated by a wave maker. Lower fluid: water (depth at rest h_1). Upper fluid: silicon oil (depth at rest h_2). Dashed lines: interface and free surface at rest. A laser vibrometer locally measures the height of the interface, the water being dyed with white paint. Inset: typical evolution of the interfacial wave height $\eta_I(t)$ as a function of time. $h_2 = 0.9$ cm.

Fig. 2: Standard deviation of the interface wave height *vs.* the upper fluid depth at rest, h_2. Solid line is from eq. (5) with $f = 4.5$ Hz, $\eta_S = 1.9$ mm, mode $+$. Top inset: typical vertical velocity of surface waves, $h_2 = 0$. Bottom inset: same for interface waves, $h_2 = 2$ mm. Wave steepness: 0.08.

turbulence theory on different wave systems (*e.g.*, hydrodynamics, optics, hydro-elastic or elastic waves) [22].

In this paper, we study gravity-capillary wave turbulence on the interface of a two-layer fluid with free upper surface. Waves propagate both at the interface and at the free surface (either in phase or in antiphase), and this coupling depends strongly on the upper fluid depth. When this depth increases, we show that these two modes become progressively uncoupled explaining thus most of the observations on the wave turbulence spectra. When the upper fluid is deep enough, the two modes are then fully uncoupled, leading to the observation of a spectrum of purely capillary interfacial wave turbulence on two decades in frequency, fluids being of almost the same density. The article is organized as follows. We will first describe the experimental setup, then the experimental results and the model, before comparing them to each other.

Experimental setup. – The experimental setup is sketched in fig. 1. Two fluids are placed in a circular 22 cm diameter plastic vessel. The lower fluid is water, and the upper fluid is a silicon oil (PDMS Dow Corning 200) [23]. Their depths at rest are, respectively, h_1 and h_2. $h_1 = 4.3$ cm is fixed, whereas h_2 is varied between 0 and 0.9 cm, thus $0 \leq h_2/h_1 < 21\%$. Their kinematic viscosities are, respectively, $\nu_1 = 10^{-6}$ m^2/s and $\nu_2 = 10^{-5}$ m^2/s. Their densities are, respectively, $\rho_1 = 1000$ kg/m^3 and $\rho_2 = 935$ kg/m^3 [24] leading to a small Atwood number $A = (\rho_1 - \rho_2)/(\rho_1 + \rho_2) = 0.033$. The surface tension of silicon oil/air is $\gamma_S = 20$ mN/m [25]. The interfacial tension between water and silicon oil is $\gamma_I = 25$ mN/m [26].

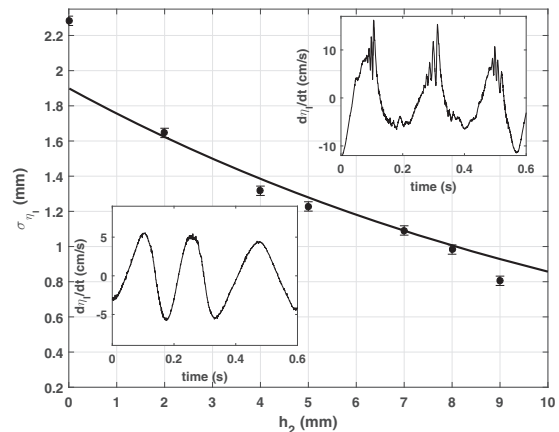An electromagnetic shaker (LDS V406/PA 100E) vibrates horizontally a plexiglas blade that generates gravity-capillary waves at the interface between both fluids and at the free surface. The immersed part of the blade is fixed to 2 cm regardless of h_2. The shaker is driven with a random forcing in amplitude and frequency between 1 Hz and 6 Hz. The rms amplitude and velocity of the blade is fixed to, respectively, 5 mm and 5 cm/s, regardless of the experiment presented here. A homemade velocity sensor [27] is fixed to the shaker axis to measure the instantaneous blade velocity $V(t)$. The interface wave steepness ranges from 0.11 to 0.04 when h_2 is decreased.

A laser Doppler vibrometer (Polytec OFV506) placed above the setup measures the vertical velocity of the interface deformation at one point given by the position of the vertical laser beam (see fig. 1). To wit, a white liquid dye (TiO$_2$ particles plus a binding agent)[1] is added to the water bulk to make it slightly diffusing (typically 1% in volume). The surface tension of dyed water/air is $\gamma_w = 32$ mN/m [28]. The velocity is extracted from the interference between the incident beam and the light backscattered by the diffusing fluid. After temporal integration, one thus obtains the interface height $\eta_I(t)$. The laser Doppler vibrometer has a sensitivity of order of 10 μm. The free surface motions being dynamics, the angle of refraction of the laser within the upper fluid will change with respect to a free surface at rest. For our weak surface wave steepnesses (< 0.13), these changes correspond to horizontal displacements of the laser on the diffuse interface less than the beam diameter on the interface (0.5 mm). To avoid direct transmitted vibration from the shaker to the vibrometer, the latter is mechanically uncoupled from the shaker. Signals are then high-pass filtered (> 0.5 Hz) to avoid possible residual low-frequency vibrations. They are acquired for $T = 5$ minutes (or 30 minutes to converge statistics to compute the probability density
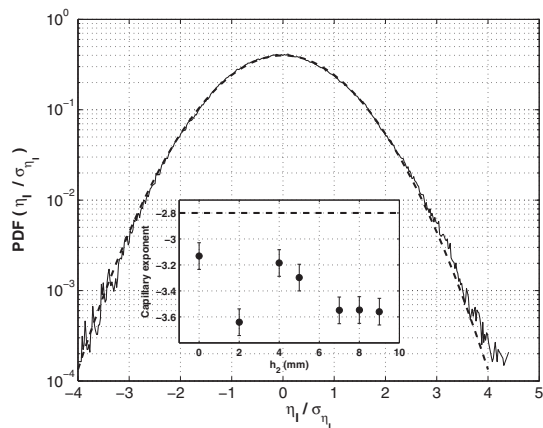
---

[1] Richard Colorants SA, Color 2000 + Blanc.

Fig. 3: Solid line: probability density function (PDF) of the rescaled interfacial wave height, η_I/σ_{η_I}. Dashed line: Gaussian with zero mean and unit standard deviation. $h_2 = 4$ mm. $\sigma_{\eta_I} = 1.32$ mm. Inset: frequency-power law exponents of the capillary spectrum as a function of h_2. Dashed line: theoretical value $-17/6$ for capillary wave turbulence.

Fig. 4: (Color online) Power spectrum density of the interface wave height, $S_{\eta_I}(f)$, for increasing upper fluid depths $h_2 = 0, 4, 5, 7, 8$ and 9 mm (from bottom to top, shifted vertically for clarity). The dashed (respectively, dash-dotted) lines are the best power-law fits of the capillary (respectively, gravity) wave turbulence regime. Forcing frequencies ≤ 6 Hz (represented by the shaded area). Inset: experimental crossover frequency f_t between gravity and capillary regimes $vs.$ h_2 (symbols). Dashed line: theoretical crossover frequency f_{c+S} (see text). Solid line: frequency f_{un} for which the interface and free surface waves of the mode $+$ become uncoupled (i.e., $\eta_I/\eta_S = 1/10$ —see fig. 7).

function (PDF) of the wave height). Surface tensions involved here are of close values: oil/air $\gamma_S = 20$ mN/m [25], water/oil $\gamma_I = 25$ mN/m [26], and dyed water/air $\gamma_w = 32$ mN/m [28]. No significative change is thus expected in the model below when using water/oil interfacial tension instead of the unknown dyed water/oil one.

Experimental results. – A temporal recording of the interfacial wave height $\eta_I(t)$ is shown in the inset of fig. 1. It displays an erratic behavior in response to the stochastic forcing. As shown in fig. 2, the standard deviation of the temporal recording of the interface wave height $\sigma_{\eta_I} \equiv \sqrt{\langle \eta_I^2(t) \rangle}$ is found to decrease strongly when the depth of the upper fluid, h_2, is increased. Temporal average is denoted by $\langle \cdot \rangle$. This experimental decrease is well described theoretically by the model presented below (solid line in fig. 2). We observe no perforation of the top layer regardless its depth. No break slope on the vertical velocity of the interfacial waves occurs that would be related on a change of index of refraction if perforation occurred. The vertical velocity is shown in the insets of fig. 2. For a single fluid ($h_2 = 0$), capillary wave generations are observed near the crests of steep gravity-capillary waves, whereas this effect is absent for a two-layer fluid ($h_2 \neq 0$). The probability density function of the rescaled interface wave height, η_I/σ_{η_I}, is close to a Gaussian (see fig. 3), and is found to be independent of h_2 (not shown).

From the temporal recording of the interface wave height, $\eta_I(t)$ (see inset of fig. 1), one computes its power spectrum density as the square modulus of the Fourier transform of $\eta_I(t)$ over a duration T: $S_{\eta_I}(f) \equiv |\int_0^T \eta_I(t)e^{i\omega t}dt|^2/(2\pi T)$, where $\omega = 2\pi f$. Figure 4 shows the power spectra of the interface wave height when the upper fluid depth increases. For $h_2 = 0$ mm (bottom curve), the usual gravity-capillary wave turbulence
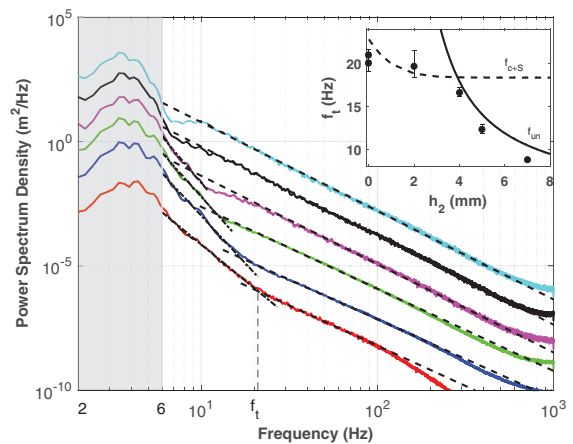
spectrum is observed as previously found in several recent studies [29–33]. Up to a cutoff frequency at ≈ 100 Hz, related to dissipation, this spectrum is consistent with two different power-law regimes for frequencies above $f_t \approx 20$ Hz (capillary regime) and below f_t (gravity regime) as expected by the weak turbulence theory [16,17] and already observed experimentally [29–33]. Note that the exponent of the capillary regime is slightly lower than its predicted value $-17/6$ (inset of fig. 3). The crossover frequency f_t between gravity and capillary wave turbulent regimes is linked to the capillary length $l_{cw} = \sqrt{\gamma_w/\rho_1 g}$ [29]. When h_2 is increased, the capillary regime is found to hold down to lower and lower frequencies (see curves from $h_2 = 4$ to 7 mm in fig. 4), until no transition is clearly visible before reaching the forcing frequencies (see curves for $h_2 \geq 8$ mm). This crossover frequency f_t is found to decrease up to a factor 2.5 (from 20 to 8 Hz, see inset of fig. 4) when h_2 is increased. Moreover, the cut-off frequency increases of a factor 7 (roughly from 100 to 700 Hz) when h_2 is increased. This leads to a significant extension of the inertial range of the capillary spectrum by more than one order of magnitude. A frequency power-law spectrum is then clearly observed on almost two decades. In the next part, we will explain the widening of the spectrum inertial range and the dependence of the crossover frequency on the upper fluid depth.

Theoretical description. – To interprete our experimental results, we consider gravity-capillary waves propagating at both the interface and the free surface of two
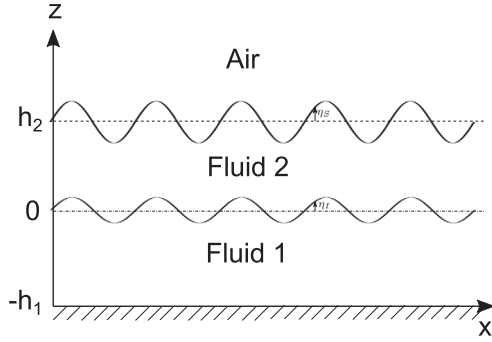
Fig. 5: Sinusoidal gravity-capillary waves propagating at the interface and at the free surface of two fluids of finite depths (h_1 and h_2 at rest). The upper surface is free. Case of in-phase deformations (mode +).

immiscible fluids of finite depths, the upper surface being free (fig. 5). The lower fluid is assumed to never emerge from the upper one. The dispersion relation of theses waves can be found in text-books [34,35] but only when the capillary effects are neglected. To our knowledge, the theoretical derivation of the dispersion relation taking into account both the gravity and capillary effects for a two-layer fluid of finite depths with free upper surface were obtained only recently [1,13], as well as the one taking also into account the fluid viscosity effects [10]. In the following, we will use the inviscid dispersion relation. The experimental validity of this hypothesis will be checked *a posteriori* (see below).

Let a sinusoidal wave propagate along the x-axis with angular frequency ω and wave vector k at the interface between both fluids, denoted 1 and 2, of finite depths (fig. 5). Fluid 1 is limited at the bottom by a rigid wall and fluid 2 is free at its surface. Experimentally, one has $6 \leq kh_1 \leq 500$ and $0.2 \leq kh_2 \leq 103$. Let η_I be the wave height at the interface and η_S be the wave height at the free surface. The system is assumed invariant along the y-axis, and the flows incompressible and inviscid. The interface at rest is located at $z = 0$. The corresponding dispersion relation reads [1,13]

$$a\omega^4 + b\omega^2 + c = 0 \qquad (1)$$

with

$$
\begin{cases}
a = \rho_2 \left[\rho_1 + \rho_2 \tanh(kh_1)\tanh(kh_2)\right], \\
b = -\rho_1(\rho_2 gk + \gamma_S k^3)\tanh(kh_2) \\
\quad + \rho_2 \left(-\rho_1 gk - (\gamma_I + \gamma_S)k^3\right)\tanh(kh_1), \\
c = \left[\gamma_I \gamma_S k^6 + g\left(\rho_2(\gamma_I - \gamma_S) + \rho_1 \gamma_S\right)k^4 \right. \\
\quad \left. -\rho_2(\rho_2 - \rho_1)g^2 k^2\right]\tanh(kh_1)\tanh(kh_2).
\end{cases}
\qquad (2)
$$

Note that for $h_1 = h_2 = \infty$, eqs. (1) and (2) are well reduced to the usual gravity-capillary dispersion relation between two infinite fluids with no free surface [35],

$$\omega^2(k) = \frac{\rho_1 - \rho_2}{\rho_1 + \rho_2}gk + \frac{\gamma_I k^3}{\rho_1 + \rho_2}. \qquad (3)$$

For $\rho_2 = 0$ and $h_2 = \infty$, eqs. (1) and (2) lead to the usual gravity-capillary dispersion relation at the free surface of a single fluid of finite depth [34],

$$\omega^2(k) = \tanh(kh_1)(gk + \gamma_I k^3/\rho_1). \qquad (4)$$

The dispersion relation in the general case, eqs. (1) and (2), has 4 solutions $\omega^2(k) = \frac{-b \pm \sqrt{b^2 - 4ac}}{2a}$ among which only 2 are real, that are plotted in solid lines (blue and red) in fig. 6. We will call these solutions "mode +" and "mode −" according to the sign in the above expression of $\omega^2(k)$. Note that the mode + has a higher phase velocity than the mode − (semilog-y plot in fig. 6). Figure 6 also shows that even for a thin enough upper fluid layer (as small as 2 mm), the wave dispersion relation is constituted of two branches corresponding to the two propagating modes. This differs strongly from the dispersion relation for interfacial waves between two infinite fluids (see dashed line) or for surface waves on the surface of a single infinite fluid (see dash-dotted line). The interfacial and free surface waves are indeed not independent but are coupled to each other by those two propagative modes. Both modes propagate at both interface and free surface. The ratio between the wave heights at the free surface (S) and the interface (I) reads [1]

$$
\frac{\eta_S}{\eta_I} = \frac{\sinh(kh_2)}{\rho_2} \times \left[\rho_2 \coth(kh_2) + \rho_1 \coth(kh_1) \right.
$$
$$
\left. - \frac{[(\rho_1 - \rho_2)g + \gamma_I k^2]k}{\omega^2(k)}\right]. \qquad (5)
$$

If $\eta_S/\eta_I > 0$, the waves at the interface and the ones at the free surface propagate in phase, corresponding to the mode + (also called barotropic [9] or zigzag [10] mode) as illustrated in fig. 5. For $\eta_S/\eta_I < 0$, they propagate in antiphase corresponding to the mode − (also called varicose mode [10]).

The modulus of the wave height ratio $|\eta_I/\eta_S|$ is plotted in fig. 7 as a function of the wave frequency for different depths h_2, for both modes. We first note that the surface wave height is higher than that of the interfacial wave height for the mode +, regardless of h_2. On the other hand, for the mode −, the interfacial wave height is higher than that of the surface wave height, regardless of h_2. Second, within our experimental inertial range ($f \geq 6$ Hz) and for small h_2, wave heights at the interface and at the free surface are found to be of the same order for both modes, and are thus coupled (see insets of fig. 7). For large h_2, waves are uncoupled since the interface wave height is much smaller (respectively, much higher) than that of the surface wave height for mode + (respectively, mode −): waves can be thus considered to propagate only at the free surface for the mode + and only at the interface for the mode −. Note that this decoupling is as strong as the wave frequency is large. These features are shown in insets of fig. 7 for a fixed frequency. Experimentally, the paddle forces both interfaces in phase at large scales, thus
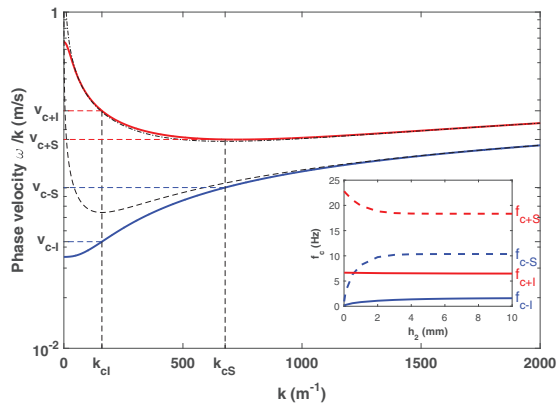
Fig. 6: (Color online) Theoretical dispersion relation ω/k vs. k for gravity-capillary waves in a two-layer fluid of finite depths from eqs. (1) and (2). Red line: in-phase mode (mode +). Blue line: antiphase mode (mode −). $h_2 = 2\,\text{mm}$. Black dashed line: dispersion relation at the interface between the same two fluids but for infinite depths (eq. (3)). Black dash-dotted line: dispersion relation at the free surface of a single fluid (2) of infinite depth (eq. (4) with $h_1 = \infty$, replacing ρ_1 and γ_I by ρ_2 and γ_S, respectively). Inset: solid (respectively, dashed) line: crossover frequencies between capillary and gravity wave regimes at the interface (respectively, at the free surface) for both modes as a function of h_2. Mode +: red. Mode −: blue.

favoring the in-phase mode. However, a mixing between the two eigenmodes occurs in practice due to the random feature of the forcing.

Interpretation. – Let us introduce the typical capillary lengths of the interface, l_{c_I}, and of the free surface, l_{c_S}. The corresponding wave numbers are $k_{c_I} \equiv 1/l_{c_I} = \sqrt{(\rho_1 - \rho_2)g/\gamma_I}$ and $k_{c_S} \equiv 1/l_{c_S} = \sqrt{\rho_2 g/\gamma_S}$ ($\lambda_{c_I} \equiv 2\pi/k_{c_I} \simeq 3.9\,\text{cm}$; $\lambda_{c_S} \equiv 2\pi/k_{c_S} \simeq 0.9\,\text{cm}$). Using the dispersion relation $\omega(k)$, those typical lengths correspond to 2 frequencies per mode: f_{c-I}, f_{c-S} (mode −) and f_{c+I}, f_{c+S} (mode +) as displayed in fig. 6 in the phase velocity space ($v \equiv \omega/k$; k) for a fixed depth h_2. Those frequencies correspond to the crossover frequencies between gravity and capillary wave regimes either at the interface (I) or at the free surface (S) for both modes (+ or −). The evolutions of these 4 frequencies with the upper fluid depth, h_2, are plotted in the inset of fig. 6. They are almost independent of h_2 within our experimental range ($h_2 \geq 2\,\text{mm}$) and only f_{c+S} and f_{c-S} lie within our experimental inertial range ($f \geq 6\,\text{Hz}$). f_{c+S} corresponds to the minimum of the upper branch of the dispersion relation (see fig. 6) except for small h_2. Moreover, the two modes are best studied when the densities of the two fluids differ slightly [1], as in our study. Indeed, $l_{c_S}/l_{c_I} = \sqrt{(\gamma_s/\gamma_i)(\rho_1 - \rho_2)/\rho_2}$. Thus, when the density difference decreases (or the interfacial tension increases), the gap between the capillary lengths will increase, but it does not modify qualitatively the results reported here.

Let us now interpret the experimental evolution of the crossover frequency f_t between gravity and capillary wave
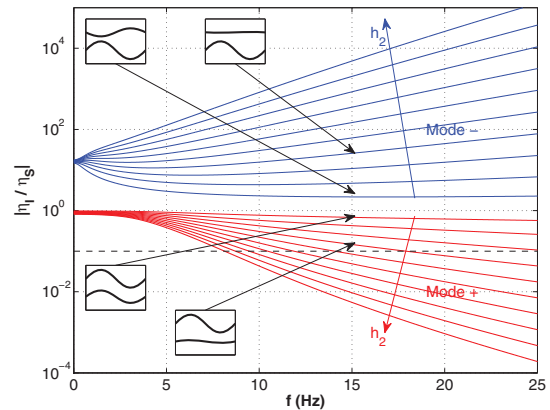

Fig. 7: (Color online) Theoretical ratio from eq. (5) between the interfacial and surface wave heights as a function of their frequencies, for different upper fluid depth $h_2 = 1$ to $10\,\text{mm}$ with a step of $1\,\text{mm}$ (see arrows). Red lines: mode +. Blue lines: mode −. Dashed line: $|\eta_I| = |\frac{\eta_S}{10}|$. Insets show temporal evolutions of the surface and interfacial wave heights, for a fixed frequency $f = 15\,\text{Hz}$, $h_2 = 1$ or $4\,\text{mm}$, and for both modes.

turbulence regimes when h_2 is increased (see inset of fig. 4). As explained above, for small depths h_2, waves at the interface and at the free surface are coupled for both propagating modes + or −. The theoretical crossover frequency f_{c+S} at the free surface for the mode + is found to well describe the data for small enough depths h_2 (see dashed line in the inset of fig. 4). When h_2 is increased, this is no longer the case. Indeed, as also explained above, when h_2 is increased, the waves propagating at the interface and at the free surface become progressively uncoupled for both modes: their relative height $|\eta_I/\eta_S|$ decreases strongly for the mode + or strongly increases for mode − (see fig. 7). We arbitrary decide that waves become uncoupled when $|\eta_I/\eta_S| \leq 1/10$ in the mode +, that is when the interface wave height becomes 10 times smaller than the free surface wave height. Interfacial waves can thus only propagate significantly on the other mode (mode −). This criterion corresponds to the dashed line in fig. 7. The intercepts of this dashed line and each solid line in fig. 7, for each depth h_2, thus give the frequencies f_{un} for which the interface and free surface waves of the mode + become uncoupled. f_{un} is then found to decrease with h_2 in rough agreement with the experimental crossover frequency f_t at large h_2 (see solid line in the inset of fig. 4).

To sum up, for small fluid depths h_2, the interface waves (that we measure) propagate on both modes and are coupled with surface waves. The crossover frequency between the gravity and capillary wave turbulence regimes observed on the spectrum, f_t, is linked to the value of f_{c+S}, the capillary length at the free surface of the in-phase mode (mode +). The dependence of f_t on h_2 is thus well described by $f_{c+S}(h_2)$ until the interfacial and surface waves decouple for large enough h_2, that is for $f_{un} < f_{c+S}$ (see inset of fig. 4).

Wave dissipation. – Let us now explain why the cut-off frequency of the wave spectrum increases strongly when an upper fluid is added. For a single fluid ($h_2 = 0$), there are three distinct mechanisms for the dissipation of wave energy: wave breaking, viscous damping and the generation of parasitic capillaries near steep crests of longer waves. Here, no wave breaking (*i.e.*, multi-valued interface) occurs since the wave steepnesses are small enough. Wave energy extraction by generation of high-frequency parasitic capillaries is indeed observed on the wavefront face as shown in the top inset of fig. 2, with a typical frequency ranging from 100 to 200 Hz. The latter comes from a resonance condition, $c_{gc} = c_c$, matching phase speeds between longer gravity-capillary waves (c_{gc}) and the shorter parasitic capillary waves (c_c) [36]. Using this condition and the dispersion relation of a single fluid, one finds a typical frequency of order of 200 Hz for ripples propagating at the same phase speeds as the longer waves near the forcing scales ($f \sim 5$ Hz). This typical frequency gives also the typical dissipative scale which is found to be in good agreement with the frequency cut-off of the wave turbulence spectrum (see fig. 4 for $h_2 = 0$). This dissipative scale depends theoretically slightly on the wave steepness [36]. In the presence of an upper layer of fluid ($h_2 \neq 0$), the resonance condition with the full dispersion relation (eqs. (1) and (2)) leads to a parasitic capillary frequency near 300 Hz (for mode +) regardless of h_2 (no solution for the mode −). However, the amplitude η_I of this parasitic capillaries is predicted to be negligible ($\eta_I < 10 \, \mu$m) regardless of h_2 by using eq. (5) with $f = 300$ Hz and assuming $\eta_S \sim 1$ mm. Indeed, experimentally for a two-layer fluid, we observe no generation of parasitic capillaries near steep crest waves as shown in the bottom inset of fig. 2. Note that this absence of parasitic capillaries should not be confused with the effect of an oil monolayer on the ocean calming gravity-capillary waves which is due to the Marangoni dissipation [37]. Thus, the main wave dissipation in our two-layer fluid system is the viscous dissipation occurring at higher frequency.

Time-scale separation. – Let us now consider the typical time scales involved in our experiment. The weak turbulence theory assumes a time-scale separation $\tau_l(f) \ll \tau_{nl}(f) \ll \tau_d(f)$, between the linear propagation time, τ_l, the nonlinear interaction time, τ_{nl}, and the dissipation time, τ_d. The linear propagation time is $\tau_l = 1/\omega(k)$. The dissipative time scale is linked to the viscous surface boundary layer, modeled by an inextensible infinitely thin film on the free surface, reading $\tau_d = \frac{2\sqrt{2}}{k(\omega)\sqrt{\nu\omega}}$ [35,38]. The kinematic viscosity of the two-layer fluid is $\nu = \frac{\mu_1 \coth(kh_1) + \mu_2 \coth(kh_2)}{\rho_1 \coth(kh_1) + \rho_2 \coth(kh_2)}$ with μ_1 (respectively, μ_2) the dynamic viscosity of the fluid beneath (respectively, above) the interface [39]. We show in fig. 8 that the condition $\tau_l(f) \ll \tau_d(f)$ is well satisfied in our experimental frequency range for both modes. It thus validates *a posteriori* the use here of an inviscid dispersion relation. Finally, for the wave turbulence to take place, the typical time scale
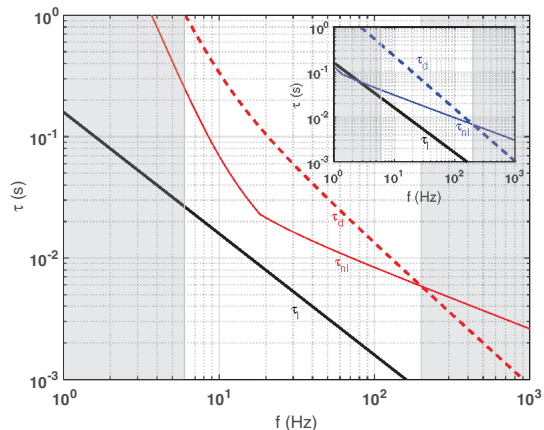

Fig. 8: (Color online) Typical time scales as a function of the wave frequency. Thick solid line: $\tau_l = 1/\omega$. Thin solid line: τ_{nl}. Dashed line: τ_d. Mode +. $h_2 = 4$ mm. Shaded areas: forcing and dissipative scales. Inset: same for mode −.

τ_{nl} of nonlinear wave interactions has to satisfy $\tau_l(f) \ll \tau_{nl}(f) \ll \tau_d(f)$. For capillary waves, $\tau_{nl} = \xi_c k^{-3/4}$ [21,40] while for gravity waves, $\tau_{nl} = \xi_g k^{-3/2}$ [40]. Since the constants ξ_c and ξ_g are experimentally unknown, τ_{nl} is plotted in fig. 8 assuming τ_{nl} to be continuous at the experimental crossover frequency, f_t, between gravity and capillary regimes, and $\tau_{nl}(f_{\text{cut}}) = \tau_d(f_{\text{cut}})$ at the cut-off frequency of the experimental capillary power-law spectrum ($f_{\text{cut}} \simeq 200$ Hz for $h_2 = 4$ mm —see fig. 4). Figure 8 shows that the time-scale separation is valid on the whole inertial range of our experiment (between shaded areas). This time-scale separation is also valid regardless of the upper fluid depth h_2.

Conclusion. – We studied gravity-capillary wave turbulence on the interface between two immiscible fluids with free upper surface. Waves propagate both at the interface and at the free surface (either in phase (mode +) or in antiphase (mode −)), and this coupling depends strongly on the upper fluid depth. When this depth is increased, these two modes become progressively uncoupled, and we show that this decoupling explains most of the observations on the wave turbulence spectra. Indeed, the crossover frequency between the gravity and capillary wave turbulence regimes is experimentally found to decrease by more than a factor 2 when the upper fluid depth is increased. At small depths, interfacial and surface waves are coupled, and this crossover is linked to the value of the capillary length at the free surface of the in-phase mode. At large enough depth, they become uncoupled when the interfacial wave heights of this mode become negligible with respect to the surface wave heights. Interfacial waves (that we measure) can thus only propagate significantly on the other mode. The crossover frequency is then well described by this decoupling criterion depending on the upper fluid depth. Finally, when the upper fluid is deep enough, the two modes are then fully uncoupled. This leads to the observation of a spectrum of purely capillary

interfacial wave turbulence on two decades in frequency, fluids being of almost the same density. This frequency range is comparable to what was previously observed at the interface between two immiscible deep fluids of almost equal densities with no upper free surface [41] or during microgravity experiments with a single fluid [42].

To our knowledge, we report the first experimental study of wave turbulence in a two-layer fluid system with free upper surface. The interface wave steepness is weak enough to reach a weak wave turbulence regime involving a linear coupling between the two propagative modes. The linear dispersion relation of this system being only derived recently, we validated it experimentally (from the depth-dependence of the crossover frequency between the gravity and capillary wave turbulence regimes). In the future, we plan to increase the wave steepness to study nonlinear coupling between modes in the wave turbulence context. To wit, a simultaneous measurement of the surface and interface elevations will be also performed. Finally, this study may be useful to better understand nonlinear wave dynamics within a two-layer fluid in the presence of surface and interfacial tensions such as oil spilling in oceanography and gravity-capillary solitary waves. The reported phenomenon is more general and should be shown in other wave turbulence systems involving the coupling between surface and interfacial waves.

$* * *$

REFERENCES

[1] MOHAPATRA S. C., KARMAKAR D. and SAHOO T., *J. Eng. Math.*, **71** (2011) 253.
[2] JAMALI M., SEYMOUR B. and LAWRENCE G. A., *Phys. Fluids*, **15** (2003) 47.
[3] EKMAN V. W., *On dead water*, in *The Norwegian North Polar Expedition 1893–1896: Scientific Results*, edited by NANSEN F., Vol. **V**, No. 15 (Publisher J. Bybwad, Christiania) 1904, pp. 1–152.
[4] MERCIER M. J., VASSEUR R. and DAUXOIS T., *Nonlin. Processes Geophys.*, **18** (2011) 193.
[5] GRUE J., *Phys. Fluids*, **27** (2015) 082103.
[6] STAPLETON N. R., in *1995 International Geoscience and Remote Sensing Symposium, IGARSS '95*, Vol. **3** (IEEE) 1995, p. 1646.
[7] WEI G., LU D. and DAI S., *Acta Mech. Sinica*, **21** (2005) 24.
[8] TROWBRIDGE J. H. and TRAYKOVSKI P., *J. Geophys. Res. Oceans*, **120** (2015) 5698.
[9] PUCCI G., BEN AMAR M. and COUDER Y., *J. Fluid Mech.*, **725** (2013) 402.
[10] POTOTSKY A. and BESTEHORN M., *Phys. Rev. Fluids*, **1** (2016) 023901.
[11] POTOTSKY A., BESTEHORN M., MERKT D. and THIELE U., *J. Chem. Phys.*, **122** (2005) 224711.
[12] PÉRON N., BROCHARD-WYART F. and DUVAL H., *Langmuir*, **28** (2012) 15844.
[13] WOOLDENDEN H. C. and PARAU E. I., *J. Fluid. Mech.*, **688** (2011) 528.
[14] KOROBKIN A., PARAU E. I. and VANDEN-BROECK J.-M., *Phil. Trans. R. Soc. A*, **369** (2011) 2803.
[15] FALCON E., *Discrete Contin. Dyn. Syst. Ser. B*, **13** (2010) 819.
[16] ZAKHAROV V. E., LVOV V. and FALKOVICH G., *Kolmogorov Spectra of Turbulence I: Wave Turbulence* (Springer-Verlag, Berlin) 1992.
[17] NAZARENKO S., *Wave Turbulence* (Springer, Berlin) 2011.
[18] NEWELL A. C. and RUMPF B., *Annu. Rev. Fluid Mech.*, **43** (2011) 59.
[19] HASSELMANN K., *J. Fluid. Mech.*, **12** (1962) 481.
[20] BENNEY D. J. and NEWELL A. C., *J. Math. Phys.*, **46** (1967) 363.
[21] ZAKHAROV V. E. and FILONENKO N. N., *J. Appl. Mech. Tech. Phys.*, **8** (1967) 37.
[22] SHRIRA V. and NAZARENKO S. (Editors), *Advances in Wave Turbulence*, Vol. **83** (World Scientific, Singapore) 2013.
[23] Dow Corning, *Safety data sheet of DMS* (2016).
[24] ATC, *Safety data sheet of PDMS* (2012) (in French).
[25] ISSENMANN B., WUNENBURGER R., CHRAIBI H., GANDIL M. and DELVILLE J.-P., *J. Fluid. Mech.*, **682** (2011) 460.
[26] ZHOU H., YAO Y., CHEN Q., LI G. and YAO S., *Appl. Phys. Lett.*, **103** (2013) 234102.
[27] FALCON E., AUMAÎTRE S., FALCÓN C., LAROCHE C. and FAUVE S., *Phys. Rev. Lett.*, **100** (2008) 064503.
[28] HERBERT E., MORDANT N. and FALCON E., *Phys. Rev. Lett.*, **105** (2010) 144502.
[29] FALCON E., LAROCHE C. and FAUVE S., *Phys. Rev. Lett.*, **98** (2007) 094503.
[30] COBELLI P., PRZADKA A., PETITJEANS P., LAGUBEAU G., PAGNEUX V. and MAUREL A., *Phys. Rev. Lett.*, **107** (2011) 214503.
[31] DENISSENKO P., LUKASCHUK S. and NAZARENKO S., *Phys. Rev. Lett.*, **99** (2007) 014501.
[32] ISSENMANN B. and FALCON E., *Phys. Rev. E*, **87** (2013) 011001(R).
[33] DEIKE L., MIQUEL B., GUTIÉRREZ P., JAMIN T., SEMIN B., BERHANU M., FALCON E. and BONNEFOY F., *J. Fluid Mech.*, **781** (2015) 196.
[34] LANDAU L. and LIFSHITZ E., *Mécanique des fluides* (MIR) 1989, §62.
[35] LAMB L. H., *Hydrodynamics* (Cambridge University Press) 1916.
[36] FEDOROV A. V., MELVILLE W. K. and ROZENBERG A., *Phys. Fluids*, **10** (1998) 1315.
[37] ALPERS W. and HÜHNERFUSS H., *J. Geophys. Res.*, **94** (1989) 6251.
[38] DEIKE L., BERHANU M. and FALCON E., *Phys. Rev. E*, **85** (2012) 066311.
[39] KUMAR K. and TUCKERMAN L. S., *J. Fluid Mech.*, **279** (1994) 49.
[40] DEIKE L., PhD Thesis (Univ. Paris Diderot) 2013.
[41] DÜRING G. and FALCÓN C., *Phys. Rev. Lett.*, **103** (2009) 174503.
[42] FALCÓN C., FALCON E., BORTOLOZZO U. and FAUVE S., *EPL*, **86** (2009) 14002.